Geophysical Research Letters

RESEARCH LETTER
10.1029/2023GL106971

A Survey of Magnetic Field Line Curvature in Jovian Dawn Magnetodisc

W. D. Gu[1,2], Z. H. Yao[1,2,3], Y. Wei[1,2], T. S. Qin[4], B. Z. Zhang[4], Y. Xu[1,2], W. R. Dunn[3], P. A. Delamere[5], and Y. N. Chen[6]

[1]Key Laboratory of Earth and Planetary Physics, Institute of Geology and Geophysics, Chinese Academy of Sciences, Beijing, China, [2]College of Earth and Planetary Sciences, University of Chinese Academy of Sciences, Beijing, China, [3]Department of Physics and Astronomy, University College London, London, UK, [4]Department of Earth Sciences, University of Hong Kong, Hong Kong, China, [5]Geophysical Institute, University of Alaska Fairbanks, Fairbanks, AK, USA, [6]Department of Earth and Space Sciences, Southern University of Science and Technology, Guangdong, China

Abstract The Jovian magnetosphere is highly dynamic, influenced by both solar wind and internal processes associated with the rapid planetary rotation and Io's volcanic activities. Accompanying the mass and energy circulations driven by the magnetospheric dynamics, the magnetic configuration also changes dramatically. One of the crucial parameters to characterize the magnetic configuration is magnetic field line curvature (FLC), which generally describes how stretched the field line is. The curvature is pivotal to influence particle behaviors, for example, pitch angle scattering which may lead to auroral particle precipitation. In this work, a method is proposed to investigate the real-time magnetic FLC in Jovian current sheet using the magnetic field data from the Juno spacecraft. The results indicate that the FLC scattering of ions and relativistic electrons are common in Jovian magnetosphere, providing a crucial insight to understand the particle behaviors.

Plain Language Summary Both the Earth and the Jupiter have intrinsic magnetic field. When the planetary magnetic field interacts with the solar wind, a region called magnetosphere is formed. Particle behaviors in different planetary systems are different, due to the different magnetospheric dynamics. The curvature of magnetic field, describing the stretch level of a magnetic field line, is a basic parameter to describe a planetary space system, and it can significantly influence particle behaviors, for example, to scatter the magnetospheric particles to planetary atmosphere, causing auroral emissions. In this work, we proposed a method to calculate the magnetic field line curvature (FLC) near the equatorial plane inside the Jupiter's magnetosphere using Juno data set, for the first time to provide a global picture on the magnetic FLC. By comparing with the radius of particles' gyration motions, we suggest that ions and electrons can be strongly scattered by the magnetic FLC. We believe that the results in this study provide useful information on the different particle behaviors between the terrestrial system and the Jovian system.

Key Points:

- We proposed a method to investigate the magnetic field line curvature (FLC) in Jupiter's current sheet using data from Juno data set
- 50 events are selected by specific criteria. The magnetic FLC and different particles' Larmor radius are investigated
- The FLC will scatter ions and relativistic electrons as a potential cause of auroral precipitation

Correspondence to:
Z. H. Yao and Y. Wei,
z.yao@mail.iggcas.ac.cn;
weiy@mail.iggcas.ac.cn

Citation:
Gu, W. D., Yao, Z. H., Wei, Y., Qin, T. S., Zhang, B. Z., Xu, Y., et al. (2024). A survey of magnetic field line curvature in Jovian dawn magnetodisc. *Geophysical Research Letters*, *51*, e2023GL106971. https://doi.org/10.1029/2023GL106971

Received 26 OCT 2023
Accepted 10 DEC 2023

Author Contributions:
Conceptualization: W. D. Gu, Z. H. Yao
Formal analysis: W. D. Gu, Z. H. Yao, B. Z. Zhang
Investigation: W. D. Gu, Z. H. Yao, Y. Wei, T. S. Qin, B. Z. Zhang, Y. Xu, Y. N. Chen
Methodology: W. D. Gu
Supervision: Z. H. Yao, Y. Wei
Visualization: W. D. Gu
Writing – original draft: W. D. Gu
Writing – review & editing: W. D. Gu, Z. H. Yao, Y. Wei, T. S. Qin, B. Z. Zhang, Y. Xu, W. R. Dunn, P. A. Delamere, Y. N. Chen

1. Introduction

The solar wind interacts with the terrestrial magnetic field forming a region called magnetosphere, which is mainly controlled by the solar wind dynamics through processes well described by Dungey (1961). Magnetospheres formed in Jovian and Kronian systems are different from the terrestrial system on the inner processes, including the large corotating magnetic field and Io's (or Enceladus') geological activities (Bagenal, 2007; Connerney et al., 2020; Delamere, 2015; Krupp et al., 2015; Smith et al., 1974; Van Allen et al., 1974; Vasyliunas, 1983). In terrestrial system, the magnetic field is dragged and forms an elongated magnetotail with a current sheet (CS) around the equatorial plane inside the magnetotail (Artemyev & Zelenyi, 2013; Ness, 1965; Speiser & Ness, 1967). In Jovian system, a CS present in all local times which may be embedded in the magnetodisc is also formed, as a consequence of internal processes, for example, centrifugal force and internal plasma sources (Achilleos, 2018; A. V. Artemyev et al., 2014; Bagenal, 2007; Delamere, 2015; Van Allen et al., 1974). Although the formation mechanisms and characteristics of CS are different in different planetary systems, the energy release processes from these planetary CSs can cause many common perturbations in planetary spaces and atmospheres, such as aurora (Bonfond et al., 2021; Kronberg et al., 2009; Lui, 1996, 2009; Ni et al., 2016; Z. H. Yao et al., 2022), magnetic reconnection (Angelopoulos et al., 2013; Arridge et al., 2016; L. J. Chen et al., 2008; Guo et al., 2018; Øieroset et al., 2001) and plasma instabilities (Lui et al., 1991; Pu et al., 1997, 1999).

Accompanying the mass and energy circulations in Jovian system, which are thought to be a combination of Vasyliunas cycle (Vasyliunas, 1983) and Dungey cycle, the magnetic configuration also undergoes dynamical changes and modulations (e.g., Kronberg et al., 2009). Magnetic field line curvature (FLC) is a basic parameter to describe the magnetic configuration. For example, the FLC in the center of CS is crucial to indicate the thickness of neutral sheet (Shen et al., 2003) and estimate the growth rate of some plasma instabilities like ballooning instability (Pu et al., 1997, 1999). Moreover, FLC is a key physical parameter to assess the particle scattering effects. When the radius of FLC is on a similar scale to the particle's Larmor radius, the particle motion becomes nonadiabatic and pitch angle diffusion occurs (Basu & Rowlands, 1986; Birmingham, 1982, 1984; Büchner & Zelenyi, 1989; J. Chen, 1992; Chirikov, 1979, 1984; West et al., 1978), which is called FLC scattering (Yu et al., 2020; Zhu et al., 2021). Strong chaos occurs when the ratio of Larmor radius to the radius of FLC is larger than 0.2 but almost vanishes when the ratio is larger than 10,000, and quasi-adiabaticity with weak chaos arises when the ratio is larger than 1 (Büchner & Zelenyi, 1989). Hence, the scale ratio (the ratio of Larmor radius to the radius of FLC) larger than 0.2 shall be a key concern in understanding the particle behaviors in planetary magnetospheres as both strong chaos and weak chaos may cause FLC scattering, and sometimes can be a reason for the auroral particle precipitation, especially the heavy energetic ions with large gyro-radii (Ni et al., 2016; Yu et al., 2020; Zhu et al., 2021).

FLC has been widely investigated in the terrestrial magnetosphere using multi-spacecraft data (Rogers et al., 2023; Saito et al., 2011; Shen et al., 2003; Y. C. Zhang et al., 2016) and in the inner and middle regions of Jupiter's magnetosphere using data from Voyager 1 and Juno (Mauk & Krimigis, 1987; Mauk et al., 2022; Paranicas et al., 1991) and the magnetospheric model (Birmingham, 1982, 1984). The observation-based investigation of FLC in the outer region of Jupiter's magnetosphere is rarely proposed so far. The main cause of pitch angle diffusion (into the loss cone) is thought to be waves against FLC scattering in the inner and middle regions of Jupiter's magnetosphere (Mauk et al., 2022), while the main cause of it in the outer regions remain uncertain. To comprehensively understand the magnetic structure and particle behaviors in Jupiter's magnetosphere, we proposed a method based on Minimum Variation Analysis (MVA) (Lepping & Behannon, 1980; Sonnerup & Scheible, 1998) and Harris model (Harris, 1962) to obtain FLC in Jupiter's CS using data from Juno Magnetic Field investigation (MAG) (Connerney, 2022). We also discussed the potential influence of FLC scattering on the magnetospheric particles.

2. Methodology

The principal idea of this investigation is to reconstruct a two-dimensional magnetic distribution and obtain the FLC. The Juno data was first transformed into a CS coordinate using MVA (Sergeev et al., 2003; Sonnerup & Scheible, 1998) and then fitted into Harris model (Harris, 1962). By adding the normal magnetic component to the modeled magnetic field, we could obtain a two-dimensional magnetic field distribution. The change of the spacecraft's location in one crossing event is ignored because the velocity of spacecraft is much smaller than the corotation velocity of CS. The detailed steps of the methodology are described below.

1. Use MVA to identify the tangential and normal direction.
   As we mainly care about the FLC at the CS center, the chosen time interval of every event represents a passing of the spacecraft through a structure near the CS center, which may be the thin current sheet (TCS) (A. V. Artemyev et al., 2014). We didn't choose the time for passing through the whole magnetodisc which can be identified through the magnetic field data, because the structure of magnetodisc is complex and the direction of tangential and normal components may change significantly. Besides, the time interval is chosen to satisfy the criteria shown in Section 3.
2. Project the total magnetic field into the tangential and normal directions to get the tangential and normal components of magnetic field (called B_l and B_n, respectively).
3. Fit B_l into Harris model.
   The magnetic field function of Harris CS (Harris, 1962) model can be described as

$$B_f = B_0 \tanh\left(\frac{v_n(t-t_0)}{L_{\text{model}}}\right) \tag{1}$$

   where $L_{\text{model}} = \frac{L_{\text{real}}}{\tanh^{-1}(\alpha)}$, $L_{\text{real}} = v_n t_{\text{half}} \cdot L_{\text{model}}$ or L_{real} is half of the thickness of the model (confined by α) or the real structure near the CS center, respectively, instead of the thickness of the whole magnetodisc. α is a parameter indicating which part of Harris model the structure near the CS center is in, as Harris model is infinite

in space. It can be adjusted to fit the data better. t_0 is the time when the spacecraft is at the CS center, which is identified by the reversal of B_l. If t_0 is in the center of the time duration, B_0 is obtained as the average of B_l at the start and end times and t_{half} is half of the time duration. If the time duration from starting time to t_0 is longer than the time duration from t_0 to ending time, B_0 is B_l at the start time and t_{half} is the time duration from starting time to t_0, or vice versa. v_n, which is the relative velocity between spacecraft and the CS in normal direction, is obtained by projecting the corotation velocity into the normal direction. The corotation velocity is estimated by the velocity of rigid corotation at $20R_j$, as the corotation velocity outside $40R_j$ suggests an asymptotic value around the velocity of rigid corotation at $20R_j$ (Frank et al., 2002; Kim et al., 2020).

4. Use the result of Harris fit (B_f) and B_n to obtain the FLC.
The FLC is given by

$$\kappa = \frac{\frac{\partial \frac{B_f}{B_n}}{\partial n}}{\left(1+\left(\frac{B_f}{B_n}\right)^2\right)^{\frac{3}{2}}} = \frac{\frac{B_0}{B_n L_{\text{model}}} \frac{1}{\cosh^2\left(\frac{v_n(t-t_0)}{L_{\text{model}}}\right)}}{\left(1+\frac{B_0^2}{B_n^2}\tanh^2\left(\frac{v_n(t-t_0)}{L_{\text{model}}}\right)\right)^{\frac{3}{2}}} \tag{2}$$

In this function, the change in B_n can be eliminated by using the constant value found at the center of CS. The FLC at the CS center which is thought to be the maximum is equal to

$$\kappa_0 = \frac{B_0}{B_n L_{\text{model}}} \tag{3}$$

The radius of FLC is defined as

$$R_c = \frac{1}{\kappa} \tag{4}$$

5. Use the ratio of the Larmor radius to the radius of FLC to show the scale ratio of a specific particle. The scale ratio is mainly used to investigate the FLC scattering under the assumption of single charge state.

The Larmor radius is given by

$$R_L = \frac{mv}{eB} = \frac{\sqrt{2mE}}{eB} \tag{5}$$

The Larmor period is given by

$$T_L = \frac{2\pi m}{eB} \tag{6}$$

where m, e, v, and E are the mass, electric quantity, velocity and energy of a charged particle, respectively. It's notable that Equation 5 isn't applicable in all circumstances. If the energy of a particle is less than $\frac{1}{2}mc^2$, which is called a nonrelativistic particle, Equation 5 is followed. m is the rest mass of the particle and c is the velocity of light in a vacuum. But if the particle's energy is larger than $\frac{1}{2}mc^2$, like an 1 MeV electron, which is called a relativistic particle, Equation 5 requires correction. In the relativistic cases we used the velocity of light in a vacuum to estimate the velocity of particle, and the relativistic effect, which makes the particle's mass larger than the rest mass, is ignored, indicating that here we focus on estimating the lower boundary of the relativistic particle's Larmor radius and Larmor period.

3. Database and Event Selection

In this study, the magnetic field data from the Juno MAG (Connerney, 2022) was examined, which has a temporal resolution of 1 s for the majority of the observing time (Connerney et al., 2017). The focus of the analysis was on the CS crossing events from November 2016 to July 2017, which occurred in the predawn sector of the outer magnetosphere, covering a wide range of radial distances from less than 50 R_j to larger than 100 R_j. Juno crossed the magnetodisc multiple times during this period, and 50 of the crossing events were well studied, employing the methodology described in Section 2. The criteria of event selection were as follows:

1. When employing MVA, three eigenvalues will be computed representing the variations in three directions, denoted as λ_1, λ_2, and λ_3, where the subscripts 1, 2, and 3 refer to maximum, intermediate, and minimum values,

respectively. The criteria for these eigenvalues were set as $\lambda_1 > 10\lambda_2$ and $\lambda_2 > 3\lambda_3$ (Lepping & Behannon, 1980; Sergeev et al., 2003).

2. The ratio of the standard deviation of Harris fit to B_0 was required to be less than 0.1.

4. Results

In this work, the MVA determination and the Harris fit are performed in each well studied event, which provides the option to use either the original data or the Harris fit for a simple two-dimensional reconstruction of the CS, as shown in Section 4.1. When calculating the FLC, using original data alone, which only uses two or three data points to estimate the FLC at a given point, may introduce unlimited errors. But if the Harris fit is used, the credibility of the result is ensured by satisfying criterion (2). Based on the results of FLC which are obtained using Harris fit, the scale ratios (the ratio of the Larmor radius to the radius of FLC) were estimated. The statistical results of all identified events are presented in Section 4.2. The FLC at the center of CS, which is thought to be the maximum in each event, can be obtained using B_n, B_0 and L_{model} only (according to Equation 3). The details of these three elements are shown in Section 4.3.

4.1. Basic Structure and Properties

A typical CS crossing event, 1 December 2016 22:58:00 to 23:07:20, was chosen to make simple reconstructions to visualize the basic structure and properties of CS (as shown in Figure 1). Using the MVA determination, we can obtain the three components of magnetic field in a CS coordinate, as described in Section 2. B_l shows a reversal of the field line's direction in CS (Figure 1a), which is also described in the Harris model. B_l combined with B_n gives two-dimensional distribution of the magnetic field in CS (Figure 1b), which enable us to investigate the FLC. Simple reconstructions were made based on the two-dimensional data (Figure 1c). The reconstruction based on B_f (Harris fit) and B_n data is slightly different from others because of the exclusion of disruptions in B_l. However, the similarity between the black and red lines near the center of CS suggests the accuracy of the analysis. The reconstruction result from B_f with B_n data is used to visualize the results of FLC, Larmor radius and scale ratio (R_L/R_c) (Figures 1d–1h) because of the confirmation of the credibility by criterion (2). At the two ends of the curve, the FLC is <0.0001 R_j^{-1} (Figure 1d), the Larmor radius of 10 keV oxygen ions is ~0.3R_j (Figure 1e), and the lower boundary of the Larmor radius of relativistic electrons is ~0.01R_j (Figure 1g). At the center of CS, the FLC is >10 R_j^{-1} (Figure 1d), the Larmor radius of 10 keV oxygen ions is ~1.5R_j (Figure 1e), and the lower boundary of the Larmor radius of relativistic electrons is ~0.05R_j (Figure 1g). The scale ratio of 10 keV oxygen ions (Figure 1f) and relativistic electrons (Figure 1h) are both >1 near the center, indicating that FLC will scatter both 10 keV oxygen ions and relativistic electrons.

4.2. Statistical Results

To provide an imaginary picture visualizing the overall characteristics, reconstruction results using B_f with B_n data (like shown in Figure 1) of all identified events were compiled together, disregarding the changes in the tangential and normal directions, as shown in Figures 2a–2c. It is revealed that the FLC at the CS center varies significantly from event to event, even at the same radial distance (Figures 2a and 2d). Several events exhibit very small or very large FLC at the CS center, with no specific limitation on the radial distances. Besides, the sizes of error bars cloud the importance of overall trend given by the average and median values (Figures 2d–2f), pointing to the complex processes in the Jupiter's magnetosphere. As for the quantitative results, the radius of FLC at the center of CS ranges mainly between 0.001R_j and 0.2R_j (Figure 2d). The Larmor radius at the center of CS ranges mainly between 0.3R_j and 10R_j (Figure 2e). And the scale ratio at the center of CS ranges mainly between 6 and 300 (Figure 2f), indicating that the FLC will commonly scatter 10 keV oxygen ions in the region near the center of CS.

4.3. B_n, B_0, and L_{model}

The FLC at the center of CS, which is thought to be the maximum of FLC in every event that we mainly cared about, can be obtained using Equation 3, which takes into account three elements: B_n, B_0, and L_{model}. The statistical results (Figures 3a–3c) and the correlations with FLC (Figures 3d–3f) of these three elements were obtained to investigate the factors influencing the FLC. Although the large standard deviations emerge in the statistical

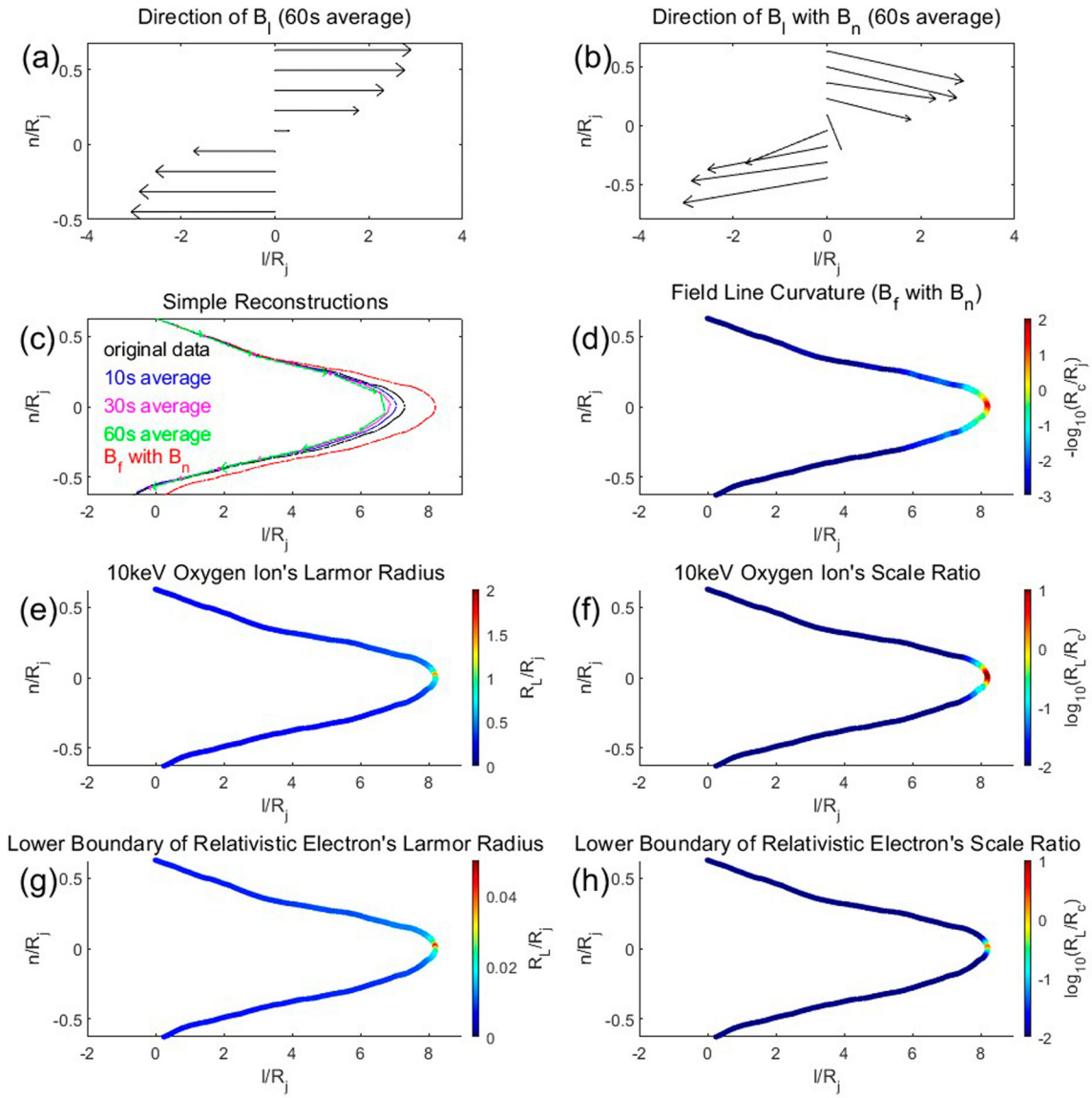

Figure 1. Simple magnetic field reconstructions of an event, 1 December 2016 22:58:00 to 23:07:20, showing the basic structure and properties of current sheet (CS). (a) The basic structure of Harris model using the 60 s average B_l data. (b) The basic structure of a two-dimensional CS using the 60 s average B_l and B_n data. (c) The field lines simply reconstructed from the original data, 10 s average data, 30 s average data, 60 s average data and B_f with B_n data, respectively. The step size of n is $\Delta n = v_n \Delta t$, and the step size of l is $\Delta l = \Delta n \bullet B_f/B_n$. Δt is the time resolution. (d) The field line curvature at every data point of the field line. (e, f) The Larmor radius and scale ratio of 10 keV oxygen ion, respectively. (g, h) The lower boundary of the Larmor radius and scale ratio of relativistic electron, respectively.

results (Figures 3a–3c), B_0 exhibits a significant decrease as the radial distance increases (Figure 3b). The corresponding trend of B_0 is similar to the results of TCS (A. V. Artemyev et al., 2014), showing that the chosen time intervals may be the crossings of TCSs. As for the correlation with FLC, both B_n (Figure 3d) and L_{model} (Figure 3f) are found to be significantly correlated with FLC. L_{model} exhibits the strongest correlation. In contrast, B_0 shows little correlation with FLC (Figure 3e). L_{model} may represent the thickness of the structure near the center of CS, as discussed in Section 2. Hence, the significant correlation between L_{model} and FLC suggests the strong dependence of FLC on the thickness of the structure near the CS center.

5. Discussion

We have investigated the FLC and the scale ratio (the ratio of the Larmor radius to the radius of FLC) of every identified event. The FLC can influence the particle's motion by FLC scattering when the scale ratio is larger

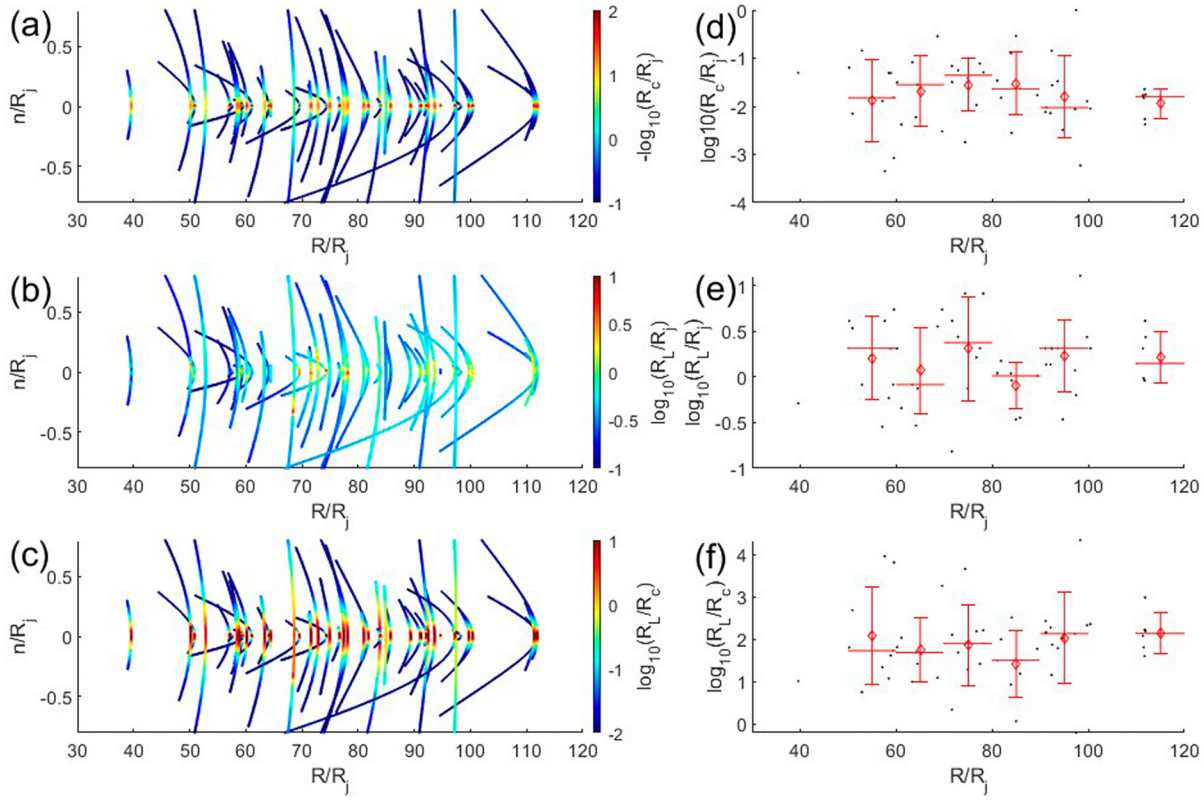

Figure 2. Reconstruction results and statistical results of all identified events. (a–c) The magnetic field line curvature (FLC), the Larmor radius of 10 keV oxygen ion and scale ratio of 10 keV oxygen ion at every data point of the field line, respectively. To avoid some extreme cases, B_n at the center of current sheet (CS) is used to be the constant B_n in every event instead of the original data. (d–f) The statistical analysis of the FLC, the Larmor radius results of 10 keV oxygen ion and the scale ratio results of 10 keV oxygen ion at the CS center of every event, respectively. The x axis is the radial distance, where R_j is estimated to be 7×10^4 km. Diamonds represent each bin's average (one bin every $10R_j$). Horizontal bars represent each bin's median. Vertical error bars are each bin's standard deviations.

than 0.2 (Büchner & Zelenyi, 1989). In the statistical results we obtained the scale ratio of 10 keV oxygen ions at CS center in every event, showing that FLC will commonly scatter 10 keV oxygen ions (Figures 2c and 2f). The Larmor radius and scale ratio of other particles can be obtained using Equation 5 and the statistical results of 10 keV oxygen ions. The scale ratio of 10 keV oxygen ions at the center of CS ranges mainly between 6 and 300, as shown in Figure 2f. Since the Larmor radius of 10 keV oxygen ions is 100 times larger than the Larmor radius of 1 eV oxygen ions, we can infer that the scale ratio of 1 eV oxygen ions at the center of CS ranges mainly between 0.06 and 3. Furthermore, for two different charged particles (with the same electric quantity), if $m_1E_1 = m_2E_2$, their Larmor radii and scale ratios will be the same at the same location (the same magnetic field). Based on this, the scale ratio of 16 eV protons and 0.5 eV sulfur ions at the center of CS can be obtained to be mainly between 0.06 and 3, and the scale ratio of 160 keV protons and 5 keV sulfur ions at the center of CS can be obtained to be mainly between 6 and 300. The lower boundary of the scale ratio of relativistic electrons at the center of CS can be obtained to be mainly between 0.18 and 9 by following the same reasoning. Additionally, according to Equation 5, the Larmor radius has positive correlation with particle's energy, which suggests the positive correlation between the scale ratio and particle's energy, as FLC remains unchanged with particle's energy. Under this conclusion we can deduce that FLC will commonly scatter oxygen ions from 1 eV to 10 keV, protons from 16 eV to 160 keV, sulfur ions from 0.5 eV to 5 keV, and relativistic electrons.

The wide existence of the phenomena of FLC scattering has been shown. But if a particle passes through the region where FLC scatters the particle in a time duration much shorter than the Larmor period, FLC scattering may have little influence on the particle's motion. Therefore, here the time durations of particles spend in this region are examined. The thickness of this region for 10 keV oxygen ions is approximately $1R_j$ (Figures 1f and 2b) and for relativistic electrons it's about $0.3R_j$ (Figure 1h). Near the center of CS, the magnetic field is estimated to be 1 nT. The Larmor period of oxygen ions is around 1×10^3 s (according to Equation 6) and the time duration

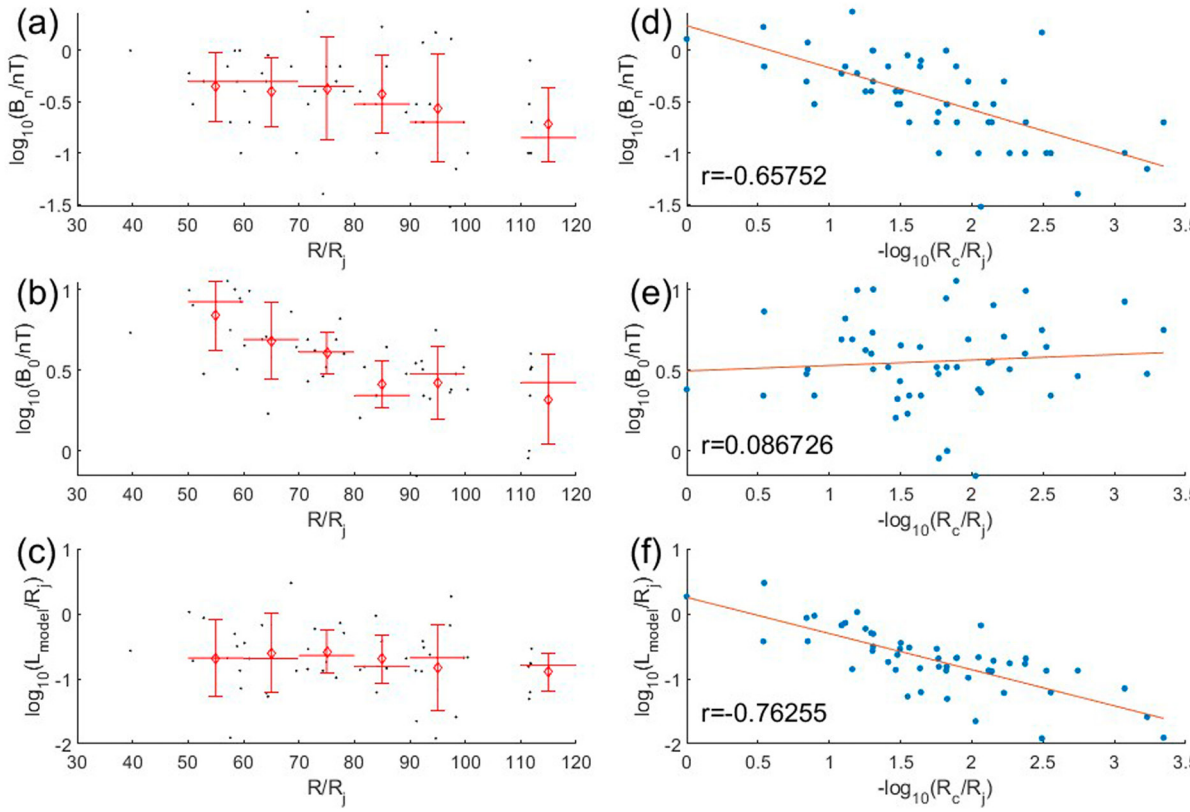

Figure 3. Statistical results and correlations with magnetic field line curvature (FLC) of the three elements used to obtain the FLC at the center of current sheet. (a–c) The statistical results of B_n, B_0, and L_{model}, respectively. The x axis is the radial distance. Diamonds represent each bin's average (one bin every $10R_j$). Horizontal bars represent each bin's median. Vertical error bars are each bin's standard deviations. (d–f) The correlations between B_n, B_0, L_{model}, and FLC, respectively. Red line in each panel is the linear least squares fit and r in each panel is the linear correlation coefficient.

for 10 keV oxygen ions to pass through $1R_j$ is longer than 2×10^2 s, which is not much shorter than the Larmor period, suggesting that FLC scattering has a noticeable influence on the motions of 10 keV oxygen ions. For relativistic electrons, the lower boundary of Larmor period is about 0.036 s and the time duration to pass through $0.3R_j$ is longer than 0.07 s, which is longer than the lower boundary of the Larmor period, indicating the FLC scattering has significant impact on the motions of relativistic electrons. As for the more energetic ions, such as 1 MeV oxygen ions, the time it takes for them to pass through this region is too short, and the large Larmor radii make the motions more complex. Wave-particle interaction may be the main cause of their diffusion instead of FLC scattering (Mauk et al., 2022).

FLC scattering plays an important role in auroral particle precipitation in the terrestrial magnetosphere (Ni et al., 2016; Yu et al., 2020; Zhu et al., 2021). This study reveals that FLC scattering widely influences the motions of ions and relativistic electrons in the predawn sector of Jupiter's CS, which suggests that it may be one of the primary sources of auroral ion precipitation. This is different from which in the inner and middle region of Jupiter's magnetosphere (Mauk et al., 2022), showing the differences between different regions. Jupiter's X-ray aurora can be generated by precipitating ions through acceleration near the auroral region (Cravens et al., 2003; Dunn et al., 2017; Metzger et al., 1983) and precipitating relativistic electrons through bremsstrahlung (Branduardi-Raymont et al., 2008). This is a potential mechanism to generate Jupiter's X-ray aurora in addition to electromagnetic waves (Z. Yao et al., 2021). The precipitation of relativistic electrons may also give rise to diffuse-like ultraviolet (UV) auroral activities, potentially in regions like the dayside "activity region" (Grodent, 2015; B. Zhang et al., 2021). But it should be noted that the main cause of UV auroras must be the discrete auroral process (Mauk et al., 2017). Besides, Jupiter's X-ray aurora is thought to have relation with cusp region (Bunce et al., 2004; Dunn et al., 2017). Therefore, ions from closed field lines generating X-ray aurora may be the evidence of the closed polar field lines found in numerical simulations (B. Zhang et al., 2021). Additionally, the CS may become thinner under the condition of solar wind compressions (Xu et al., 2023). Thinner CS

may result in smaller L_{model}. Due to the strong correlation between L_{model} and FLC (as shown in Section 4.3), the solar wind compression may cause larger FLC and subsequently more particles precipitating into auroral region. This is a potential process to generate the enhanced X-ray aurora (Dunn et al., 2016).

6. Summary

Magnetic FLC is a fundamental parameter to describe the morphology of magnetic field and can influence particle properties as the FLC scattering will occur if the scale ratio (the ratio of the Larmor radius to the radius of FLC) is larger than 0.2 (Büchner & Zelenyi, 1989). This work proposed a method to investigate the FLC in current sheet (CS) using the magnetic field data from Juno MAG (Connerney, 2022), in the predawn sector of Jupiter's outer magnetosphere. Under the criterion (1, 2), 50 crossing events were selected and examined. The FLC was investigated, and the characteristics of the particles' motions were studied. We believe the main results can help to construct a comprehensive view to the structures and particles' motions in the Jupiter's CS (e.g., A. V. Artemyev et al., 2023).

At the center of CS, the radius of FLC ranges mainly between $0.001R_j$ and $0.2R_j$, the Larmor radius of 10 keV oxygen ion ranges mainly between $0.3R_j$ and $10R_j$, the scale ratio of 10 keV oxygen ion ranges mainly between 6 and 300. The FLC exhibits strong dependence on B_n and L_{model} but little on B_0. Based on these results, the Larmor radius and scale ratio of other particles can be obtained according to Equation 5. The FLC scattering is found to widely influences the motions of various particles including oxygen ions from 1 eV to 10 keV, protons from 16 eV to 160 keV, sulfur ions from 0.5 eV to 5 keV, and relativistic electrons. The investigated time duration for particles to pass through the region affected by FLC scattering supports the wide prevalence.

The wide existence of the phenomena of FLC scattering suggests that it's a potential mechanism for the generation of the diffuse-like Jupiter's auroras in addition to electromagnetic waves (for X-ray aurora, e.g., Z. Yao et al., 2021) and Alfvenic waves (for UV aurora, e.g., Pan et al., 2020). The X-ray aurora generated by ions from closed field lines could serve as the evidence for the existence of the closed polar field lines (Dunn et al., 2017; B. Zhang et al., 2021). A potential correlation between solar wind compression and FLC increasing may lead to the enhanced X-ray aurora (Dunn et al., 2016). In future we would further study the FLC-related magnetospheric dynamics, such as plasma instabilities (e.g., ballooning instabilities) (Pu et al., 1997, 1999), and compare with auroral observations (e.g., Grodent et al., 2018) to understand the Jovian system disruptions.

Data Availability Statement

All Juno data presented here are publicly available from NASA's Planetary Data System as part of the JNO-J-3-FGM-CAL-V1.0 (https://pds-ppi.igpp.ucla.edu/search/view/?f=yes&id=pds://PPI/JNO-J-3-FGM-CAL-V1.0) dataset for the MAG instrument (Connerney, 2022).

Acknowledgments
This work was supported by the Strategic Priority Research Program of Chinese Academy of Sciences, Grant XDB 41000000. Z.Y. acknowledges the National Science Foundation of China (Grant 42074211) and Key Research Program of the Institute of Geology & Geophysics CAS (Grant IGGCAS-201904). W.R.D. acknowledges support from STFC consolidated Grant ST/S000240/1 to University College London (UCL).

References

Achilleos, N. (2018). The nature of Jupiter's magnetodisk current system. In A. Keiling, O. Marghitu, & M. Wheatland (Eds.), *Electric currents in geospace and beyond, geophysical monograph 235* (pp. 127–138). John Wiley & Sons: American Geophysical Union. https://doi.org/10.1002/9781119324522.ch8

Angelopoulos, V., Runov, A., Zhou, X. Z., Turner, D. L., Kiehas, S. A., Li, S. S., & Shinohara, I. (2013). Electromagnetic energy conversion at reconnection fronts. *Science*, *341*(6153), 1478–1482. https://doi.org/10.1126/science.1236992

Arridge, C., Eastwood, J., Jackman, C., Poh, G. K., Slavin, J. A., Thomsen, M. F., et al. (2016). Cassini in situ observations of long-duration magnetic reconnection in Saturn's magnetotail. *Nature Physics*, *12*(3), 268–271. https://doi.org/10.1038/nphys3565

Artemyev, A., & Zelenyi, L. (2013). Kinetic structure of current sheets in the earth magnetotail. *Space Science Reviews*, *178*(2–4), 419–440. https://doi.org/10.1007/s11214-012-9954-5

Artemyev, A. V., Ma, Q., Ebert, R. W., Zhang, X.-J., & Allegrini, F. (2023). Force-free current sheets in the Jovian magnetodisk: The key role of electron field-aligned anisotropy. *Journal of Geophysical Research: Space Physics*, *128*(3), e2022JA031280. https://doi.org/10.1029/2022JA031280

Artemyev, A. V., Vasko, I. Y., & Kasahara, S. (2014). Thin current sheets in the Jovian magnetotail. *Planetary and Space Science*, *96*, 133–145. https://doi.org/10.1016/j.pss.2014.03.012

Bagenal, F. (2007). The magnetosphere of Jupiter: Coupling the equator to the poles. *Journal of Atmospheric and Solar-Terrestrial Physics*, *69*(3), 387–402. https://doi.org/10.1016/j.jastp.2006.08.012

Basu, S., & Rowlands, G. (1986). Analytical treatment of charged particle motion in the geomagnetotail. *Planetary and Space Science*, *34*(7), 631–637. https://doi.org/10.1016/0032-0633(86)90040-1

Birmingham, T. J. (1982). Charged particle motions in the distended magnetospheres of Jupiter and Saturn. *Journal of Geophysical Research*, *87*(A9), 7421–7430. https://doi.org/10.1029/ja087ia09p07421

Birmingham, T. J. (1984). Pitch angle diffusion in the Jovian magnetodisc. *Journal of Geophysical Research*, *89*(A5), 2699–2707. https://doi.org/10.1029/ja089ia05p02699

Bonfond, B., Yao, Z. H., Gladstone, G. R., Grodent, D., Gérard, J.-C., Matar, J., et al. (2021). Are dawn storms Jupiter's auroral substorms? *AGU Advances*, *2*(1), e2020AV000275. https://doi.org/10.1029/2020AV000275

Branduardi-Raymont, G., Elsner, R. F., Galand, M., Grodent, D., Cravens, T. E., Ford, P., et al. (2008). Spectral morphology of the X-ray emission from Jupiter's aurorae. *Journal of Geophysical Research*, *113*(A2), 1–11. https://doi.org/10.1029/2007ja012600

Büchner, J., & Zelenyi, L. M. (1989). Regular and chaotic charged particle motion in magnetotaillike field reversals: 1. Basic theory of trapped motion. *Journal of Geophysical Research*, *94*(A9), 11821–11842. https://doi.org/10.1029/JA094iA09p11821

Bunce, E. J., Cowley, S. W. H., & Yeoman, T. K. (2004). Jovian cusp processes: Implications for the polar aurora. *Journal of Geophysical Research*, *109*(A9), 1–26. https://doi.org/10.1029/2003ja010280

Chen, J. (1992). Nonlinear dynamics of charged particles in the magnetotail. *Journal of Geophysical Research*, *97*(A10), 15011–15050. https://doi.org/10.1029/92JA00955

Chen, L.-J., Bhattacharjee, A., Puhl-Quinn, P. A., Yang, H., Bessho, N., Imada, S., et al. (2008). Observation of energetic electrons within magnetic islands. *Nature Physics*, *4*(1), 19–23. https://doi.org/10.1038/nphys777

Chirikov, B. V. (1979). A universal instability of many-dimensional oscillator systems. *Physics Reports*, *52*(5), 263–379. https://doi.org/10.1016/0370-1573(79)90023-1

Chirikov, B. V. (1984). Particle dynamics in magnetic traps. In *Topics in plasma theory (in Russian)* (Vol. 13, pp. 3–73). Energoizdat.

Connerney, J. E. P. (2022). Juno magnetometer Jupiter archive JNO-J-3-FGM-CAL-V1.0 [Dataset]. NASA Planetary Data System. https://doi.org/10.17189/1519711

Connerney, J. E. P., Benn, M., Bjarno, J. B., Denver, T., Espley, J., Jorgensen, J. L., et al. (2017). The Juno magnetic field investigation. *Space Science Reviews*, *213*(1–4), 39–138. https://doi.org/10.1007/s11214-017-0334-z

Connerney, J. E. P., Timmins, S., Herceg, M., & Joergensen, J. L. (2020). A Jovian magnetodisc model for the Juno era. *Journal of Geophysical Research: Space Physics*, *125*(10), e2020JA028138. https://doi.org/10.1029/2020JA028138

Cravens, T. E., Waite, J. H., Gombosi, T. I., Lugaz, N., Gladstone, G. R., Mauk, B. H., & MacDowall, R. J. (2003). Implications of Jovian X-ray emission for magnetosphere-ionosphere coupling. *Journal of Geophysical Research*, *108*(A12), 1–12. https://doi.org/10.1029/2003ja010050

Delamere, P. A. (2015). Solar wind interaction with giant magnetospheres and earth's magnetosphere. In *Magnetotails in the solar system, geophysical monograph* (Vol. 207, pp. 217–233). The AGU Publications Committee.

Dungey, J. W. (1961). Interplanetary magnetic field and the auroral zones. *Physical Review Letters*, *6*(2), 47–48. https://doi.org/10.1103/PhysRevLett.6.47

Dunn, W. R., Branduardi-Raymont, G., Elsner, R. F., Vogt, M. F., Lamy, L., Ford, P. G., et al. (2016). The impact of an ICME on the Jovian X-ray aurora. *Journal of Geophysical Research: Space Physics*, *121*(3), 2274–2307. https://doi.org/10.1002/2015JA021888

Dunn, W. R., Branduardi-Raymont, G., Ray, L. C., Jackman, C. M., Kraft, R. P., Elsner, R. F., et al. (2017). The independent pulsations of Jupiter's northern and southern X-ray auroras. *Nature Astronomy*, *1*(11), 758–764. https://doi.org/10.1038/s41550-017-0262-6

Frank, L. A., Paterson, W. R., & Khurana, K. K. (2002). Observations of thermal plasmas in Jupiter's magnetotail. *Journal of Geophysical Research*, *107*(A1), 1003. https://doi.org/10.1029/2001JA000077

Grodent, D. (2015). A brief review of ultraviolet auroral emissions on giant planets. *Space Science Reviews*, *187*(1–4), 23–50. https://doi.org/10.1007/s11214-014-0052-8

Grodent, D., Bonfond, B., Yao, Z., Gérard, J.-C., Radioti, A., Dumont, M., et al. (2018). Jupiter's aurora observed with HST during Juno orbits 3 to 7. *Journal of Geophysical Research: Space Physics*, *123*(5), 3299–3319. https://doi.org/10.1002/2017JA025046

Guo, R. L., Yao, Z. H., Wei, Y., Ray, L. C., Rae, I. J., Arridge, C. S., et al. (2018). Rotationally driven magnetic reconnection in Saturn's dayside. *Nature Astronomy*, *2*(8), 640–645. https://doi.org/10.1038/s41550-018-0461-9

Harris, E. G. (1962). On a plasma sheath separating regions of oppositely directed magnetic field. *Nuovo Cimento*, *23*(1), 115–121. https://doi.org/10.1007/BF02733547

Kim, T. K.-H., Ebert, R. W., Valek, P. W., Allegrini, F., McComasm, D. J., Bagenal, F., et al. (2020). Survey of ion properties in Jupiter's plasma sheet: Juno JADE-I observations. *Journal of Geophysical Research: Space Physics*, *125*(4), e2019JA027696. https://doi.org/10.1029/2019JA027696

Kronberg, E. A., Woch, J., Krupp, N., & Lagg, A. (2009). A summary of observational records on periodicities above the rotational period in the Jovian magnetosphere. *Annales Geophysicae*, *27*(6), 2565–2573. https://doi.org/10.5194/angeo-27-2565-2009

Krupp, N., Kronberg, E., & Radioti, A. (2015). Jupiter's magnetotail. In *Magnetotails in the solar system* (pp. 85–98). American Geophysical Union (AGU). https://doi.org/10.1002/9781118842324.ch5

Lepping, R., & Behannon, K. (1980). Magnetic field directional discontinuities: 1. Minimum variance errors. *Journal of Geophysical Research*, *85*(A9), 4695–4703. https://doi.org/10.1029/JA085iA09p04695

Lui, A. T. Y. (1996). Current disruption in the Earth's magnetosphere: Observations and models. *Journal of Geophysical Research*, *101*(A6), 13067–13088. https://doi.org/10.1029/96JA00079

Lui, A. T. Y. (2009). Comment on "tail reconnection triggering substorm onset". *Science*, *324*(5933), 1391. https://doi.org/10.1126/science.1167726

Lui, A. T. Y., Chang, C.-L., Mankofsky, A., Wong, H.-K., & Winske, D. (1991). A cross-field current instability for substorm expansions. *Journal of Geophysical Research*, *96*(A7), 11389–11401. https://doi.org/10.1029/91JA00892

Mauk, B. H., Allegrini, F., Bagenal, F., Bolton, S. J., Clark, G., Connerney, J. E. P., et al. (2022). Loss of energetic ions comprising the ring current populations of Jupiter's middle and inner magnetosphere. *Journal of Geophysical Research: Space Physics*, *127*(5), e2022JA030293. https://doi.org/10.1029/2022JA030293

Mauk, B. H., Haggerty, D., Paranicas, C., Clark, G., Kollmann, P., Rymer, A. M., et al. (2017). Discrete and broadband electron acceleration in Jupiter's powerful aurora. *Nature*, *549*(7670), 66–69. https://doi.org/10.1038/nature23648

Mauk, B. H., & Krimigis, S. M. (1987). Radial force balance within Jupiter's dayside magnetosphere. *Journal of Geophysical Research*, *92*(A9), 9931–9941. https://doi.org/10.1029/JA092iA09p09931

Metzger, A. E., Luthey, J. L., Gilman, D. A., Hurley, K. C., Schnopper, H. W., Seward, F. D., & Sullivan, J. D. (1983). The detection of X rays from Jupiter. *Journal of Geophysical Research*, *88*(A10), 7731–7741. https://doi.org/10.1029/JA088iA10p07731

Ness, N. F. (1965). The earth's magnetic tail. *Journal of Geophysical Research*, *70*(13), 2989–3005. https://doi.org/10.1029/JZ070i013p02989

Ni, B. B., Thorne, R. M., Zhang, X. J., Bortnik, J., Pu, Z. Y., Xie, L., et al. (2016). Origins of the earth's diffuse auroral precipitation. *Space Science Reviews*, *200*(1–4), 205–259. https://doi.org/10.1007/s11214-016-0234-7

Øieroset, M., Phan, T. D., Fujimoto, M., Lin, R. P., & Lepping, R. P. (2001). In situ detection of collisionless reconnection in the Earth's magnetotail. *Nature*, *412*(6845), 414–417. https://doi.org/10.1038/35086520

Pan, D. X., Yao, Z. H., Manners, H., Dunn, W., Bonfond, B., Grodent, D., et al. (2020). Ultralow-frequency waves in driving Jovian aurorae revealed by observations from HST and Juno. *Geophysical Research Letters*, *48*(5), e2020GL091579. https://doi.org/10.1029/2020GL091579

Paranicas, C. P., Mauk, B. H., & Krimigis, S. M. (1991). Pressure anisotropy and radial stress balance in the Jovian neutral sheet. *Journal of Geophysical Research*, *96*(A12), 21135–21140. https://doi.org/10.1029/91JA01647

Pu, Z. Y., Kang, K. B., Korth, A., Fu, S. Y., Zong, Q. G., Chen, Z. X., et al. (1999). Ballooning instability in the presence of a plasma flow: A synthesis of tail reconnection and current disruption models for the initiation of substorms. *Journal of Geophysical Research*, *104*(A5), 10248. https://doi.org/10.1029/1998JA900104

Pu, Z. Y., Korth, A., Chen, Z. X., Friedel, R. H. W., Zong, Q. G., Wang, X. M., et al. (1997). MHD drift ballooning instability near the inner edge of the near-Earth plasma sheet and its application to substorm onset. *Journal of Geophysical Research*, *102*(A7), 14397–14406. https://doi.org/10.1029/97JA00772

Rogers, A. J., Farrugia, C. J., Torbert, R. B., & Rogers, T. J. (2023). Applying magnetic curvature to MMS data to identify thin current sheets relative to tail reconnection. *Journal of Geophysical Research: Space Physics*, *128*(1), e2022JA030577. https://doi.org/10.1029/2022JA030577

Saito, M. H., Fairfield, D., Le, G., Hau, L.-N., Angelopoulos, V., McFadden, J. P., et al. (2011). Structure, force balance, and evolution of incompressible cross-tail current sheet thinning. *Journal of Geophysical Research*, *116*(A10), A10217. https://doi.org/10.1029/2011JA016654

Sergeev, V., Runov, A., Baumjohann, W., Nakamura, R., Zhang, T. L., Volwerk, M., et al. (2003). Current sheet flapping motion and structure observed by Cluster. *Geophysical Research Letters*, *30*(6), 1327. https://doi.org/10.1029/2002GL016500

Shen, C., Li, X., Dunlop, M., Liu, Z. X., Balogh, A., Baker, D. N., et al. (2003). Analyses on the geometrical structure of magnetic field in the current sheet based on cluster measurements. *Journal of Geophysical Research*, *108*(A5), 1168. https://doi.org/10.1029/2002JA009612

Smith, E. J., Davis, L., Jones, D. E., Colburn, D. S., Coleman, P. J., Dyal, P., & Sonett, C. P. (1974). The magnetic field of Jupiter and its interaction with the solar wind. *Science*, *183*(4122), 305–306. https://doi.org/10.1126/science.183.4122.305

Sonnerup, B. U., & Scheible, M. (1998). Minimum and maximum variance analysis. In *Analysis methods for multi-spacecraft data* (Vol. 1, pp. 185–220).

Speiser, T. W., & Ness, N. F. (1967). The neutral sheet in the geomagnetic tail: Its motion, equivalent currents, and field line connection through it. *Journal of Geophysical Research*, *72*(1), 131. https://doi.org/10.1029/jz072i001p00131

Van Allen, J. A., Baker, D. N., Randall, B. A., Thomsen, M. F., Sentman, D. D., & Flindt, H. R. (1974). Energetic electrons in the magnetosphere of Jupiter. *Science*, *183*(4122), 309–311. https://doi.org/10.1126/science.183.4122.309

Vasyliunas, V. M. (1983). Plasma distribution and flow. In A. J. Dessler (Ed.), *Physics of the Jovian magnetosphere* (pp. 395–453). Cambridge University Press.

West, H. I., Buck, R. M., & Kivelson, M. G. (1978). On the configuration of the magnetotail near midnight during quiet and weakly disturbed periods: Magnetic field modeling. *Journal of Geophysical Research*, *83*(A8), 3819–3829. https://doi.org/10.1029/ja083ia08p03819

Xu, Y., Yao, Z. H., Zhang, B., Delamere, P. A., Ray, L. C., Dunn, W. R., et al. (2023). On the relation between Jupiter's aurora and the dawnside current sheet. *Geophysical Research Letters*, *50*(13), e2023GL104123. https://doi.org/10.1029/2023GL104123

Yao, Z., Dunn, W. R., Woodfield, E. E., Clark, G., Mauk, B. H., Ebert, R. W., et al. (2021). Revealing the source of Jupiter's X-ray auroral flares. *Science Advances*, *7*(28), eabf0851. https://doi.org/10.1126/sciadv.abf0851

Yao, Z. H., Bonfond, B., Grodent, D., Chané, E., Dunn, W. R., Kurth, W. S., et al. (2022). On the relation between auroral morphologies and compression conditions of Jupiter's magnetopause: Observations from Juno and the Hubble Space Telescope. *Journal of Geophysical Research: Space Physics*, *127*(10), e2021JA029894. https://doi.org/10.1029/2021JA029894

Yu, Y., Tian, X., & Jordanova, V. K. (2020). The effects of field line curvature (FLC) scattering on ring current dynamics and isotropic boundary. *Journal of Geophysical Research: Space Physics*, *125*(8), e2020JA027830. https://doi.org/10.1029/2020JA027830

Zhang, B., Delamere, P. A., Yao, Z., Bonfond, B., Lin, D., Sorathia, K. A., et al. (2021). How Jupiter's unusual magnetospheric topology structures its aurora. *Science Advances*, *7*(15), eabd1204. https://doi.org/10.1126/sciadv.abd1204

Zhang, Y. C., Shen, C., Marchaudon, A., Rong, Z. J., Lavraud, B., Fazakerley, A., et al. (2016). First in situ evidence of electron pitch angle scattering due to magnetic field line curvature in the Ion diffusion region. *Journal of Geophysical Research: Space Physics*, *121*(5), 4103–4110. https://doi.org/10.1002/2016JA022409

Zhu, M., Yu, Y., Tian, X., Shreedevi, P. R., & Jordanova, V. K. (2021). On the ion precipitation due to field line curvature (FLC) and EMIC wave scattering and their subsequent impact on ionospheric electrodynamics. *Journal of Geophysical Research: Space Physics*, *126*(3), e2020JA028812. https://doi.org/10.1029/2020JA028812